JACS JOURNAL OF THE AMERICAN CHEMICAL SOCIETY

ARTICLE

pubs.acs.org/JACS

Selective Binding of O_2 over N_2 in a Redox−Active Metal−Organic Framework with Open Iron(II) Coordination Sites

Eric D. Bloch,[†] Leslie J. Murray,[†,§] Wendy L. Queen,[‖] Sachin Chavan,[⊥] Sergey N. Maximoff,[‡] Julian P. Bigi,[†] Rajamani Krishna,[#] Vanessa K. Peterson,[▽] Fernande Grandjean,[○] Gary J. Long,[◆] Berend Smit,[‡] Silvia Bordiga,[⊥] Craig M. Brown,[‖,▽] and Jeffrey R. Long[*,†]

[†]Department of Chemistry and [‡]Department of Chemical and Biomolecular Engineering, University of California, Berkeley, California 94720, United States

[§]Department of Chemistry, University of Florida, Gainesville, Florida 32611, United States

[‖]Center for Neutron Research, National Institute of Standards and Technology, Gaithersburg, Maryland 20899, United States

[⊥]Department of Inorganic, Physical, and Materials Chemistry, NIS Centre of Excellence and INSTM Centre of Reference, University of Turin, Via Quarello 11, I-10135 Torino, Italy

[#]Van't Hoff Institute for Molecular Sciences, Univeristy of Amsterdam, Science Park 904, 1098 XH Amsterdam, The Netherlands

[▽]The Bragg Institute, Australian Nuclear Science and Technology Organisation, PMB1, Menai, NSW, Australia

[○]Faculty of Sciences, University of Liège, B-4000 Sart-Tilman, Belgium

[◆]Department of Chemistry, Missouri University of Science and Technology, University of Missouri, Rolla, Missouri 65409-0010, United States

S *Supporting Information*

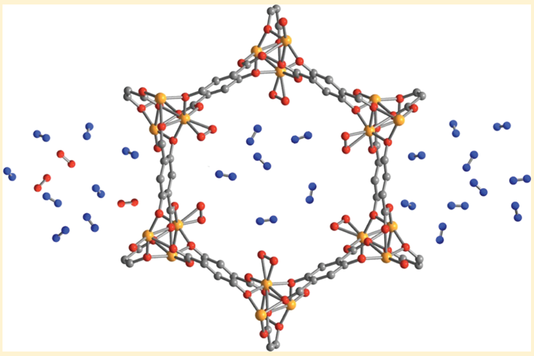

ABSTRACT: The air-free reaction between $FeCl_2$ and H_4dobdc (dobdc^{4-} = 2,5-dioxido-1,4-benzenedicarboxylate) in a mixture of *N*,*N*-dimethylformamide (DMF) and methanol affords Fe_2(dobdc)·4DMF, a metal−organic framework adopting the MOF-74 (or CPO-27) structure type. The desolvated form of this material displays a Brunauer−Emmett−Teller (BET) surface area of 1360 m^2/g and features a hexagonal array of one-dimensional channels lined with coordinatively unsaturated Fe^{II} centers. Gas adsorption isotherms at 298 K indicate that Fe_2(dobdc) binds O_2 preferentially over N_2, with an irreversible capacity of 9.3 wt %, corresponding to the adsorption of one O_2 molecule per two iron centers. Remarkably, at 211 K, O_2 uptake is fully reversible and the capacity increases to 18.2 wt %, corresponding to the adsorption of one O_2 molecule per iron center. Mössbauer and infrared spectra are consistent with partial charge transfer from iron(II) to O_2 at low temperature and complete charge transfer to form iron(III) and O_2^{2-} at room temperature. The results of Rietveld analyses of powder neutron diffraction data (4 K) confirm this interpretation, revealing O_2 bound to iron in a symmetric side-on mode with d_{O-O} = 1.25(1) Å at low temperature and in a slipped side-on mode with d_{O-O} = 1.6(1) Å when oxidized at room temperature. Application of ideal adsorbed solution theory in simulating breakthrough curves shows Fe_2(dobdc) to be a promising material for the separation of O_2 from air at temperatures well above those currently employed in industrial settings.

INTRODUCTION

With over 100 million tons produced annually, O_2 is one of the most widely used commodity chemicals in the world.[1] Its potential utility in processes associated with the reduction of carbon dioxide emissions from fossil fuel-burning power plants, however, means that the demand for pure O_2 could grow enormously. For implementation of precombustion CO_2 capture, pure O_2 is needed for the gasification of coal, which produces the feedstock for the water−gas shift reaction used to produce CO_2 and H_2.[2] In addition, oxyfuel combustion is receiving considerable attention for its potential utility as an alternative to postcombustion CO_2 capture. Here, pure O_2 is diluted to 0.21 bar with CO_2 and fed into a power plant for fuel combustion. Since N_2 is absent from the resulting flue gas, the requirement for postcombustion separation of CO_2 from N_2 is eliminated.[3]

The separation of O_2 from air is currently carried out on a large scale using an energy-intensive cryogenic distillation process.[4] Zeolites are also used for O_2/N_2 separation,[5] both industrially and in portable medical devices; however, this process is inherently inefficient as the materials used adsorb N_2 over O_2 with poor selectivity. By employing materials that selectively adsorb

Received: June 27, 2011
Published: August 10, 2011

O_2 and can operate near ambient temperatures, lower energy and capital costs could be realized. Metal−organic frameworks, which have already received considerable attention for applications in gas storage[6] and separation,[7] represent a promising new class of potential O_2 separation materials.

The high surface areas and open metal coordination sites possible within metal−organic frameworks make them particularly attractive for the development of an adsorption-based process for the separation of O_2 from air. While coordinatively unsaturated metal centers have been generated in such materials via chelation by postsynthetically modified bridging ligands,[8] or via insertion into open ligand sites,[9] they are most often created by evacuation of frameworks that have metal-bound solvent molecules. This strategy has been employed to expose M^{2+} cation sites in some of the most widely studied frameworks, such as M_2(dobdc) (M = Mg, Mn, Co, Ni, Zn; dobdc^{4-} = 2,5-dioxido-1,4-benzenedicarboxylate)[10] and $M_3(BTC)_2$ (M = Cu, Cr, Mo; BTC^{3-} = 1,3,5-benzenetricarboxylate).[11] To achieve a high selectivity for the coordination of O_2 over N_2, one can take advantage of the greater electron affinity of the former molecule. Indeed, we recently showed that the coordinatively unsaturated Cr^{II} centers in $Cr_3(BTC)_2$ give rise to an exceptionally strong preference for adsorbing O_2 relative to N_2 via charge transfer.[11c] Although the interaction with O_2 proved too strong to achieve full reversibility with this material, the result demonstrates the potential power of frameworks with redox-active metal centers for the separation of O_2 and N_2. In view of its widespread deployment as an O_2 carrier in biology,[12] Fe^{II} is an obvious candidate for such purposes.

Herein, we report the synthesis and O_2 binding properties of Fe_2(dobdc), a metal−organic framework with a high density of coordinatively unsaturated Fe^{II} centers lining the pore surface.

EXPERIMENTAL SECTION

General. Unless otherwise noted, all procedures were performed under an N_2 atmosphere using standard glovebox or Schlenk techniques. Anhydrous, air-free *N*,*N*-dimethylformamide (DMF) and methanol were purchased from commercial vendors and further deoxygenated by purging with N_2 for at least 1 h prior to being transferred to an inert atmosphere glovebox. All other reagents were obtained from commercial vendors at reagent grade purity or higher and used without further purification.

Synthesis of Fe_2(dobdc). Anhydrous ferrous chloride (1.1 g, 9.0 mmol), 1,4-dihydroxyterephthalic acid (0.71 g, 3.6 mmol), DMF (300 mL), and methanol (36 mL) were added to a 500 mL Schlenk flask. The reaction mixture was heated at 393 K and stirred for 18 h to afford a red-orange precipitate. The solid was collected by filtration and washed with 100 mL of DMF to yield 2.0 g (91%) of Fe_2(dobdc)·4DMF. Anal. Calcd. for $C_{20}H_{30}Fe_2N_4O_{10}$: C, 40.16; H, 5.06; N, 9.37. Found: C, 40.26; H, 5.08; N, 9.24. A sample of this compound (1.9 g, 3.3 mmol) was soaked in 100 mL of DMF at 393 K for 24 h after which the solvent was decanted, and the solid was then soaked in 100 mL of methanol at 343 K for 24 h. The methanol exchange was repeated three times, and the solid was collected by filtration to yield 1.25 g (87%) of Fe_2(dobdc)·4MeOH as a yellow-ochre powder. Anal. Calcd. for $Fe_2C_{12}H_{18}O_{10}$: C, 33.21; H, 4.18. Found: C, 33.42; H, 4.09. A sample of this compound was fully desolvated by heating under dynamic vacuum (<10 μbar) at 433 K for 24 h to yield Fe_2(dobdc) as a light green powder. Anal. Calcd. for $Fe_2C_8H_2O_6$: C, 31.42; H, 0.66. Found: C, 31.55; H, 0.50.

Low-Pressure Gas Adsorption Measurements. For all gas adsorption measurements 200−225 mg of Fe_2(dobdc)·4MeOH was transferred to a preweighed glass sample tube under an atmosphere of nitrogen and capped with a Transeal. Samples were then transferred to a Micromeritics ASAP 2020 gas adsorption analyzer and heated at a rate of 0.1 K/min from room temperature to a final temperature of 433 K. Samples were considered activated when the outgas rate at 433 K was less than 2 μbar/min. Evacuated tubes containing degassed samples were then transferred to a balance and weighed to determine the mass of sample, typically 150−175 mg. The tube was transferred to the analysis port of the instrument where the outgas rate was again determined to be less than 2 μbar/min at 433 K. Nitrogen gas adsorption isotherms at 77 K were measured in liquid nitrogen, while O_2 measurements between 200 and 273 K were measured using liquid nitrogen/solvent slurry baths. All measurements above 273 K were performed using a recirculating dewar connected to an isothermal bath.

Transmission Infrared and Diffuse Reflectance UV−Vis-NIR Spectroscopy. Prior to O_2 dosing, Fe_2(dobdc)·4MeOH samples were activated under dynamic vacuum (residual pressure <0.1 μbar) at 433 K for 18 h. Infrared spectra were collected on thin deposits of sample supported on a silicon wafer in an airtight quartz cell that allows for collection of spectra under controlled atmospheres. The film was prepared from a suspension of Fe_2(dobdc) in methanol. Transmission FTIR spectra were collected at 2 cm^{-1} resolution on a Bruker IFS 66 FTIR spectrometer equipped with a DTGS detector. Diffuse reflectance UV−vis-NIR spectra were recorded on a Cary 5000 spectrophotometer equipped with a reflectance sphere. Spectra of the desolvated framework were recorded on a thick self-supported wafer of the sample. Attenuated total reflection (ATR) spectra were recorded on a Bruker single reflection ALPHA-Platinum ATR spectrometer with a diamond crystal accessory.

Neutron Diffraction Data Collection and Refinement. Neutron powder diffraction (NPD) experiments were carried out on 0.9698 and 0.6200 g of Fe_2(dobdc) and $Fe_2(O_2)$(dobdc), respectively, using the high-resolution neutron diffractometer, BT1, at the National Institute of Standards and Technology Center for Neutron Research (NIST). Both samples were placed in a He purged glovebox, loaded into a vanadium can equipped with a gas loading valve, and sealed using an indium O-ring. Neutron diffraction data were collected using a Ge(311) monochromator with an in-pile 60′ collimator corresponding to a wavelength of 2.0782 Å. The samples were loaded into a top-loading closed cycle refrigerator, and then data were collected at 4 K. After data collection of the bare material, O_2 loading was then carried out. The sample was warmed to 125 K and then exposed to a predetermined amount of gas (2.0 O_2 per Fe^{2+}). Upon reaching an equilibrium pressure at the loading temperature, the sample was then slowly cooled to ensure complete adsorption of the O_2. Data was then collected at 4 K.

NPD measurements of N_2-loaded Fe_2(dobdc) were performed on the Echidna instrument[13] located at the Opal research reactor and operated by the Bragg Institute within the Australian Nuclear Science and Technology Organisation (ANSTO). A desolvated sample weighing 1.079 g was transferred to a vanadium cell in an Ar-filled glovebox. The cell was equipped with heaters for the gas line and valve to allow condensable gases to be loaded in the sample when mounted in the closed cycle refrigerator. The high-resolution diffractometer was configured with a Ge(331) monochromator using a takeoff angle of 140° with no collimation at the monochromator and fixed tertiary 5′ collimation, resulting in a wavelength of 2.4406 Å. Diffraction data were collected at ∼9 K for the evacuated framework and with sequential loadings of 0.5, 1.0, and 2.0 N_2:Fe, where the cryostat and sample were heated above 80 K to facilitate adsorption of the 99.999% pure N_2 gas.

All NPD data were analyzed using the Rietveld method as implemented in EXPGUI/GSAS.[14] The activated Fe_2(dobdc) model was refined with all structural and peak profile parameters free to vary, resulting in a structure very similar to that determined using single crystal X-ray diffraction. Fourier difference methods were then employed to locate the adsorbed molecules in the data collected from the samples subsequently loaded with O_2 or N_2. The atoms in the adsorbed molecules were modeled individually. For the N_2 adsorbed sample, the two N atoms were constrained to maintain the fractional occupancy and isotropic displacement parameter within each diatomic molecule. For analysis of $Fe_2(dobdc)$ loaded with 2.0 O_2/Fe, only fractional occupancies were constrained to maintain the same values, while all other parameters were allowed to vary. Further, for data collection of the irreversibly oxidized sample, $Fe_2(O_2)(dobdc)$, the modeled O atoms were constrained to maintain the same fractional occupancies and isotropic displacement parameters. Once a stable structural model was obtained, the isotropic displacement parameters of the adsorbed O_2 molecule were allowed to vary independently of one another and then the displacement parameters for O(1b) were allowed to refine anisotropically.

Mössbauer Spectroscopy. The Mössbauer spectra of $Fe_2(dobdc)$, $Fe_2(O_2)_2(dobdc)$, and $Fe_2(O_2)(dobdc)$ were measured at various temperatures between 45 and 298 K with a constant acceleration spectrometer which utilized a rhodium matrix cobalt-57 source, and was calibrated at 295 K with α-iron foil. The absorber contained 45(1) mg/cm^2 of powder mixed with boron nitride. The $Fe_2(dobdc)$ absorber was prepared in an N_2-filled glovebox, cooled to 77 K with liquid nitrogen, and inserted into a precooled cryostat under dry helium. The sample of $Fe_2(O_2)_2(dobdc)$ was prepared in situ by dosing the evacuated cryostat to 300 mbar O_2 at 94 K and allowing 3 h for equilibration. The sample of $Fe_2(O_2)(dobdc)$ was prepared in situ by warming the oxidized sample above 250 K in the cryostat. The spectra of $Fe_2(dobdc)$ were measured at 298, 94, and 45 K in the absence of O_2, after which the sample was warmed to 94 K and dosed with O_2. Additional spectra were measured between 94 and 298 K and then subsequently measured again at 94 and 298 K. All spectra were fit with symmetric Lorenzian quadrupole doublets; the resulting spectral parameters, listed in the order of measurement, are given in Table S3 (Supporting Information). The temperature dependence of the observed isomer shifts and relative absorption areas are plotted in Figures S12 and S13 (Supporting Information), respectively; further spectral details are provided in the Supporting Information. The relative statistical errors associated with the isomer shifts, quadrupole splittings, line widths, percent areas, and absolute areas between 94 and 298 K are also given in Table S3.

Other Physical Measurements. Thermogravimetric analysis was carried out at a ramp rate of 1 °C/min in a nitrogen flow with a TA Instruments TGA 5000 apparatus. Powder X-ray diffraction patterns were collected on air-free samples sealed in quartz capillaries on a Bruker Advance D8 powder X-ray diffractometer equipped with a capillary stage.

RESULTS AND DISCUSSION

Synthesis of $Fe_2(dobdc)$. The reaction of anhydrous $FeCl_2$ with H_4dobdc in a mixture of DMF and methanol affords a solvated form of $Fe_2(dobdc)$ as a red-orange microcrystalline powder. Powder X-ray diffraction data (see Figure S1, Supporting Information) show the compound to adopt the MOF-74 or CPO-27 structure type displayed in Figure 1, as previously reported for $M_2(dobdc)$ (M = Mg, Mn, Co, Ni, Zn).[10] The compound rapidly changes color to dark brown upon exposure to air, presumably due to at least partial oxidation of the Fe^{II} centers by O_2. Based upon color, it is likely that the brown phase previously reported as $Fe_2(dobdc)$ is actually some oxidized form of the compound.[10h] Note that, perhaps owing to their air-sensitive nature, only a very few metal–organic frameworks based upon iron(II) have yet been isolated.[15]

The new framework was completely desolvated by soaking it in methanol to exchange coordinated DMF, followed by heating under dynamic vacuum at 433 K for 48 h. The resulting solid was light green in color. Rietveld analysis of the powder neutron diffraction data collected for $Fe_2(dobdc)$ indicates retention of the framework structure with no residual bound solvent (see Figure S2, Supporting Information). Thus, desolvation converts the Fe^{II} centers of the framework from an octahedral coordination geometry with one bound solvent molecule to a square pyramidal geometry with an open coordination site.

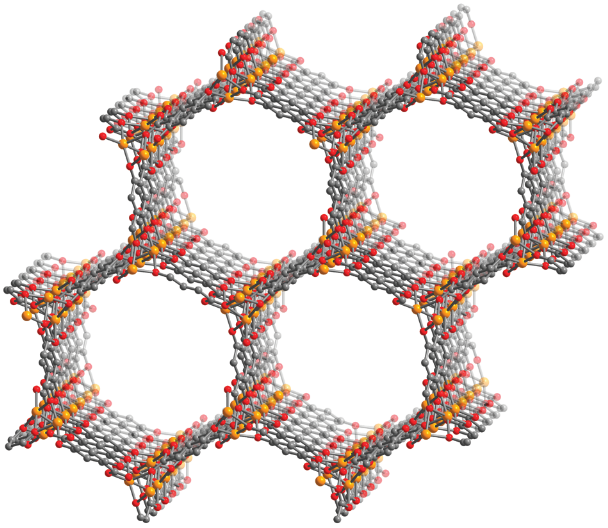

Figure 1. Portion of the crystal structure of desolvated $Fe_2(dobdc)$ as viewed approximately along the [001] direction. Orange, gray, and red spheres represent Fe, C, and O atoms, respectively; H atoms have been omitted for clarity.

Low-pressure N_2 adsorption data obtained for $Fe_2(dobdc)$ at 77 K reveal a type I adsorption isotherm characteristic of a microporous solid. The data indicate a Brunauer–Emmett–Teller (BET) surface area of 1360 m^2/g (1535 m^2/g Langmuir) (see Figure S3, Supporting Information). This value is significantly higher than the 920 m^2/g Langmuir surface area reported for the material prepared in the presence of air and is in close agreement with the BET surface areas of 1218 and 1341 m^2/g reported for $Ni_2(dobdc)$ and $Co_2(dobdc)$, respectively, indicating full evacuation of solvent molecules from the pores of the material.[16]

UV–Vis-NIR Spectroscopy. Figure 2 shows the electronic absorption spectra for $Fe_2(dobdc)\cdot 4MeOH$, $Fe_2(dobdc)$, and H_4dobdc. The spectrum for the yellow-ochre compound $Fe_2(dobdc)\cdot 4MeOH$ exhibits a low energy doublet with peaks at 11 600 and 7600 cm^{-1}. High-spin Fe^{II} centers in an octahedral symmetry are expected to show a spin-allowed transition, $^5E_g \leftarrow {}^5T_{2g}$, in the near-infrared region,[17] and in many compounds this band is split into a doublet due to a lower symmetry ligand field, which lifts the twofold orbital degeneracy of the ^5E_g term. At higher energy, a broad component centered at 16 000 cm^{-1} and a strong band with a maximum around 21 000 cm^{-1} appear in the spectrum. The structure and position of these absorptions suggest they arise from mixing of d–d and charge transfer (LMCT and MLCT) transitions.[18] Heating the solvated material at 433 K in vacuo results in removal of coordinated methanol with the formation of five-coordinate Fe^{II} centers. The corresponding change in symmetry at the metal site to approximately C_{4v} strongly affects the electronic transitions, as is evident from the spectrum of the desolvated material. In particular, the band at 21 000 cm^{-1} slightly shifts to lower energy, mixing with the component at 16 000 cm^{-1} and with the d–d transition, resulting in a strong absorption extending through 13 000 cm^{-1}. The very strong

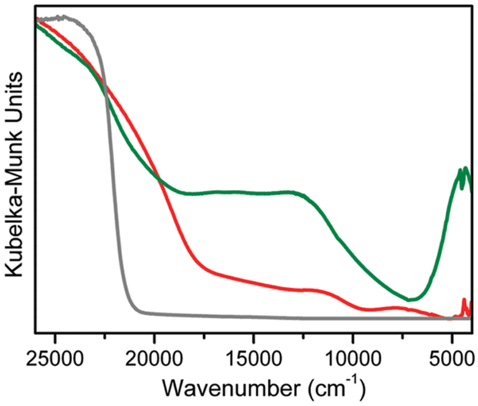

Figure 2. Diffuse reflectance UV−vis-NIR spectra of methanol solvated (red) and desolvated (green) Fe_2(dobdc) and H_4dobdc (gray).

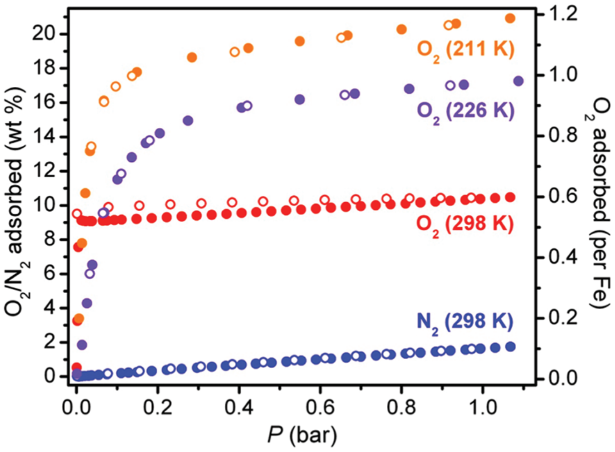

Figure 3. Excess O_2 adsorption isotherms collected for Fe_2(dobdc) at 211 (orange), 226 (purple), 298 K (red) and N_2 adsorption at 298 K (blue). Filled and open circles represent adsorption and desorption, respectively.

absorption maximum at 4400 cm^{-1} is associated with a d−d transition, with enhanced intensity owing to loss of an approximate inversion center in the ligand field upon conversion from pseudooctahedral to square pyramidal coordination.

O_2 and N_2 Adsorption. Gas adsorption isotherms indicate that Fe_2(dobdc) preferentially binds O_2 over N_2 at all temperatures measured (201, 211, 215, 226, and 298 K). As shown in Figure 3, the O_2 adsorption isotherm measured at 298 K is extremely steep, climbing to near 9.3 wt % at a pressure of just 0.01 bar. As the pressure is increased to 1.0 bar, uptake increases slightly to 10.4 wt %. The steep initial rise in the isotherm is consistent with strong binding of O_2 to some of the Fe^{II} centers, while the subsequent gradual increase in adsorption is likely due to O_2 physisorbed to the framework surface. Importantly, the amount of strongly bound O_2 corresponds to 0.5 molecules per iron center. Adsorption of N_2 under these conditions is noticeably lower, gradually rising to just 1.3 wt % at 1.0 bar. The selectivity factor of this material, calculated as the mass of O_2 adsorbed at 0.21 bar divided by the mass of N_2 adsorbed at 0.79 bar, is 7.5. Although this selectivity factor is among the highest reported for metal−organic frameworks,[19] room temperature O_2 adsorption was found to be irreversible. Attempts to identify conditions to release coordinated O_2 by heating at temperatures of up to 473 K under dynamic vacuum ultimately lead to decomposition of the framework.

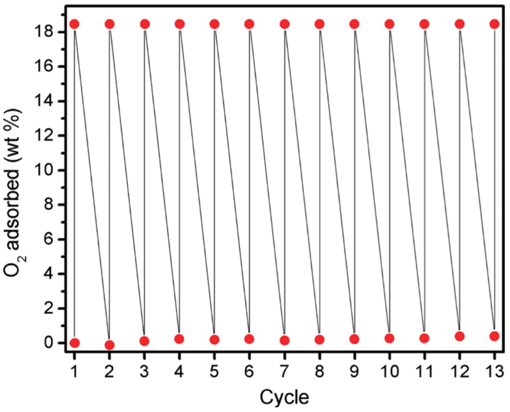

Figure 4. Uptake and release of O_2 in Fe_2(dobdc) over 13 cycles at 211 K. Adsorption occurred within 2 min upon application of 0.21 bar of O_2, and desorption was carried out by placing the sample under dynamic vacuum for 25 min.

Upon dosing Fe_2(dobdc) with O_2 at lower temperatures, it was noted that the black color characteristic of the oxidized framework could be returned to light green by applying vacuum to the sample, suggesting reversible O_2 adsorption. Additional O_2 adsorption experiments confirmed this result. As shown in Figure 3, at 226 K, the framework adsorbs 14.1 wt % O_2 at 0.21 bar, or 0.82 O_2 molecules per iron site. Although adsorption at this temperature is largely reversible, O_2 uptake decreases to 11.9 wt % after four adsorption/desorption cycles. Lowering the adsorption temperature to 211 K results in an increased O_2 uptake of 18.2 wt %, corresponding to 1.0 molecules of O_2 per iron center. The amount of O_2 adsorbed at this temperature was found to decrease only slightly to 17.5 wt % after eight adsorption/desorption experiments. However, cycling at a rapid rate, allowing just 2 min for adsorption and 25 min for desorption (instead of the 4−5 h typically required for collecting a full isotherm), resulted in no noticeable loss in adsorption capacity after 13 cycles (see Figure 4).

To predict how Fe_2(dobdc) would perform as an O_2/N_2 separation material, ideal adsorbed solution theory (IAST) was employed at temperatures for which O_2 adsorption is reversible. The O_2 and N_2 isotherms measured at 201, 211, 215, and 226 K were modeled with dual-site Langmuir−Freundlich fits (see Figure S5, Supporting Information). Isosteric heats of adsorption calculated from these fits are plotted in Figure S6 (Supporting Information) and indicate higher enthalpies for O_2 adsorption than N_2 adsorption over the entire pressure range measured. The higher propensity of O_2 to accept charge from Fe^{II} results in a larger initial isosteric heat of −41 kJ/mol, as compared to that of N_2 (−35 kJ/mol). Accordingly, Fe_2(dobdc) displays a high O_2/N_2 selectivity at 201, 211, 215, and 226 K. As shown in Figure S7 (Supporting Information), the selectivity ranges from 4.4 to over 11 and reaches a maximum of 11.4 at 201 K and about 0.4 bar.

The high O_2/N_2 selectivity in conjunction with the rapid and reversible cycling times, suggests that Fe_2(dobdc) warrants further consideration as an adsorbent for O_2/N_2 separations via a modified vacuum-swing adsorption (VSA) process (see Figure S8, Supporting Information). Here, dry air is flowed over a packed bed of Fe_2(dobdc) at temperatures near 210 K, which could potentially offer significant cost and energy savings over current separation technologies that are performed at much lower temperatures. Breakthrough experiments were simulated

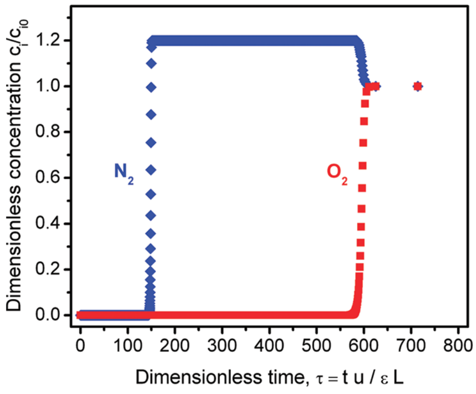

Figure 5. Calculated N_2 (blue diamonds) and O_2 (red squares) breakthrough curves during adsorption of simulated air (O_2:N_2 = 0.21:0.79) by Fe_2(dobdc) at 211 K.

at 211 and 226 K to evaluate the performance of Fe_2(dobdc) for the separation of O_2 from N_2 at concentrations similar to those present in air (see Figure 5). The methodology adopted for the breakthrough simulations has been described in detail elsewhere.[20] The *x*-axis in Figure 5 is a dimensionless time, τ, obtained by dividing the actual time, *t*, by the contact time between the gas and metal−organic framework crystallites, $\varepsilon L/u$. For a given adsorbent, under selected operating conditions, the breakthrough characteristics are uniquely defined by τ, allowing the results presented here to be equally applicable to laboratory scale equipment as well as to industrial scale adsorbers. It is apparent from the simulated curves that N_2 quickly saturates the sample, as evidenced by the low breakthrough time. The mol % of N_2 in the outlet stream as a function of dimensionless time is presented in Figure S9 (Supporting Information). In contrast to currently employed VSA processes, in which N_2 is selectively adsorbed on the packed bed while O_2 is collected, Fe_2(dobdc) would selectively adsorb O_2.[21] Accordingly, shortly after N_2 breakthrough, the gas stream is pure nitrogen while O_2 is retained by the framework. Upon O_2 breakthrough, the VSA process is advanced to the second step, in which vacuum is applied to the sample bed. Although the gas at the outlet is initially a mixture of N_2 and O_2, the concentration of O_2 quickly increases to near 100 mol % (see Figure S9, Supporting Information). This results in a large supply of pure O_2. After a majority of the O_2 is removed from the adsorber, a low-pressure flow of pure N_2 would be flowed over the material to fully regenerate the bed for subsequent cycling.

Mössbauer Spectra. The different O_2 adsorption behavior at low versus room temperature suggests the existence of two different modes by which O_2 binds to the open iron sites in Fe_2(dobdc). Mössbauer spectroscopy was employed to probe the electronic structure at the metal center. At all temperatures, the spectra of Fe_2(dobdc) in the absence of O_2 feature a simple doublet. At 298 K, this doublet exhibits an isomer shift of 1.094(3) mm/s and a quadrupole splitting of 2.02(1) mm/s. These values are consistent with high-spin iron(II) in a square pyramidal coordination environment, as established below for the structure of the compound. Upon exposure to O_2, a small amount (ca. 5−15%, depending upon temperature) of high-spin iron(II) is still observed, presumably because a small portion of the iron(II) sites remain unoxygenated.

As shown in Figure 6, the spectrum obtained in the presence of O_2 at 94 K indicates that almost all of the iron in the sample has a substantially reduced isomer shift that is approximately halfway between those expected for high-spin iron(II) and high-spin iron(III). This suggests a partial transfer of electron density from each of the Fe^{II} centers in the framework to form a weak bond with an O_2 species that is somewhere between the neutral molecule and superoxide. Thus, exposure of Fe_2(dobdc) to O_2 at low temperatures is consistent with the formation of $Fe_2(O_2)_2$(dobdc), featuring one weakly held O_2 molecule per iron atom. This is fully consistent with the observation of a reversible adsorption of 18.2 wt % O_2 at 211 K. At this point, it is not possible to determine from the Mössbauer spectral results whether the electron transfer is static or dynamic, with an electron transfer time that is faster than the ca. 10^{-7} s time scale of the iron-57 Mössbauer spectral experiment.

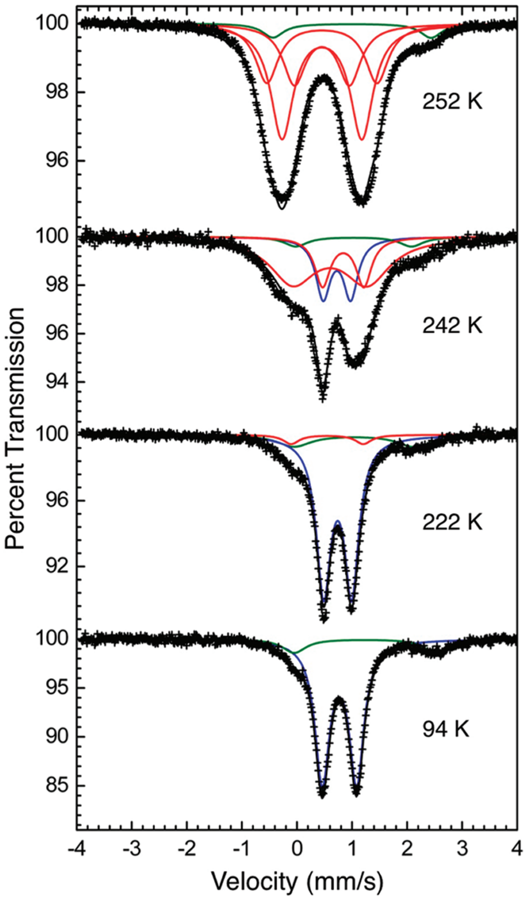

Figure 6. Mössbauer spectra measured between 94 and 252 K for Fe_2(dobdc) in the presence of O_2. The green doublet is attributed to high-spin Fe^{II}, while the blue doublet corresponds to high-spin $Fe^{II/III}$ with partial charge transfer to bound O_2. The red spectral components are attributed to high-spin Fe^{III} with differing environments, one of which presumably corresponds to the O_2^{2-}-bound species.

Upon warming to 222 K and above, further changes arise in the Mössbauer spectra, which are clearly indicative of the formation of high-spin iron(III). The temperature at which this change in oxidation state occurs is consistent with the temperature at which we first observe the onset of and irreversible uptake of O_2 in gas adsorption experiments (ca. 220 K). The change in oxidation state together with the irreversible uptake of 9 wt % O_2 suggests the formation of a compound of formula $Fe_2(O_2)$(dobdc), in which half of the Fe^{III} centers strongly bind a peroxide anion. Note that, consistent with the presence of at least two different coordination environments, one with

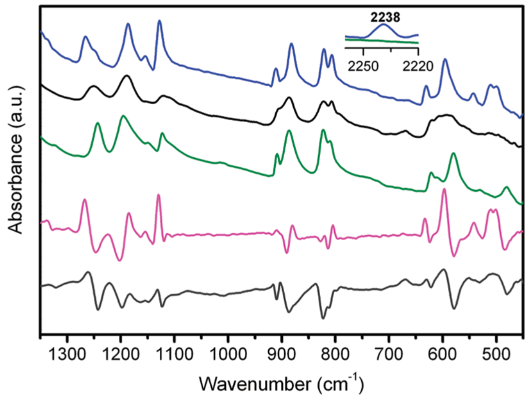

Figure 7. Infrared spectra obtained for Fe_2(dobdc) in the absence of O_2 at room temperature (green) and upon dosing with 30 mbar of O_2 at room temperature (black) and at a low temperature near 100 K (blue). Difference spectra between the bare and O_2-dosed materials at low and room temperature are shown in magenta and gray, respectively.

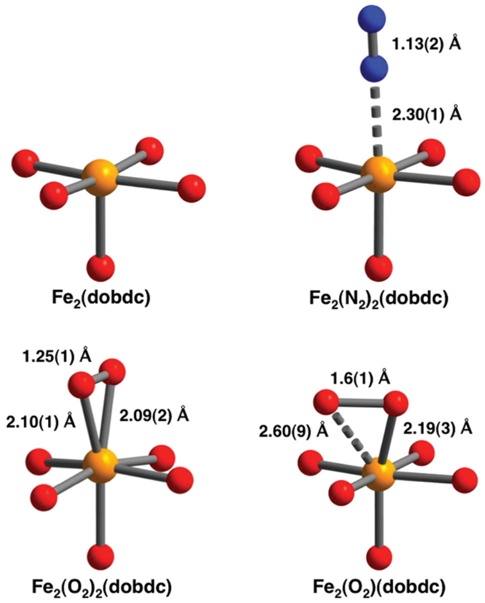

Figure 8. First coordination spheres for the iron centers within Fe_2(dobdc) and its O_2 and N_2 dosed variants, as determined from Rietveld analysis of neutron powder diffraction data. Orange, blue, and red spheres represent Fe, N, and O atoms, respectively. The structures depicted are for samples under vacuum (upper left), dosed with N_2 at 100 K (upper right), dosed with O_2 at 100 K (lower left), and dosed with O_2 at 298 K (lower right). All diffraction data were collected below 10 K. Values in parentheses give the estimated standard deviation in the final digit of the number.

O_2^{2-} bound and one without, fitting the spectra requires the use of at least two doublets for the iron(III) components.

The temperature dependence of the quadrupole splitting of the main spectral components observed for the framework in the presence of O_2, corresponding to the Fe^{II} centers in Fe_2(dobdc), the $Fe^{II/III}$ centers in $Fe_2(O_2)_2$(dobdc), and the Fe^{III} centers in $Fe_2(O_2)$(dobdc), is shown in Figure S10 (Supporting Information). As expected and in agreement with the Ingalls model,[22] the quadrupole splitting of the square pyramidal high-spin Fe^{II} center in Fe_2(dobdc) decreases the most with increasing temperature, a decrease that results from changes in the electronic population of the $3d_{xy}$, $3d_{xz}$, and $3d_{yz}$ orbitals, whose degeneracy has been removed by the low-symmetry component of the crystal field. Furthermore, there is a smaller decrease in the splitting upon warming of the other two components. The temperature dependence of the logarithm of the Mössbauer spectral absorption area of Fe_2(dobdc) (see Figure S11, Supporting Information) is well fit with the Debye model for a solid[23] and yields a Debye temperature, Θ_D, of 225(7) K, a value that is reasonable for the compound. Overall, the Mössbauer data point to a situation where, as a sample of Fe_2(dobdc) is warmed under O_2, an activation barrier is overcome for the transfer of electrons from two different iron centers to form a bound peroxide anion at every other iron site.

Infrared Spectra. The presence of various Fe—O_2 adducts as a function of temperature should also be apparent by infrared spectroscopy. Spectra collected in transmission mode on thin films of Fe_2(dobdc) (see Figure 7, green) reveal a number of framework vibrations below 1300 cm^{-1}. The reactivity of Fe_2(dobdc) toward O_2 was followed at both room temperature and near 100 K. The series of spectra obtained near 100 K with varying O_2 loadings are shown in Figure S14 (Supporting Information). Oxygenation of Fe_2(dobdc) at low temperature gives rise to the blue spectrum in Figure 7, and the most relevant changes are evident in the difference spectrum shown in magenta. New bands are seen at 1129, 541, and 511 cm^{-1}, while significant shifts are seen in the framework bands originally at 1250, 1198, and 580 cm^{-1} (causing negative components in the difference spectrum). The component at 1129 cm^{-1} is assigned to υ(O—O) of a partially reduced (near superoxo) O_2 species coordinated to $Fe^{II/III}$ sites. The first overtone for this stretching mode is also clearly visible at 2238 cm^{-1}. The band at 541 cm^{-1} is associated with the Fe—O_2 vibration of this species, whereas the band at 511 cm^{-1} is attributed to an Fe—O_{linker} mode of the framework, reflecting the O_2 adsorption induced modification in Fe—O_{linker} bonds.[24] The interaction with O_2 at low temperature is completely reversible by applying vacuum to the sample cell.

Oxygenation of Fe_2(dobdc) at room temperature gives rise to the black spectrum depicted in Figure 7, which can be explained in terms of the formation of a peroxo species coordinated to Fe^{III} centers.[25] The main features in this case are a peak at 790 cm^{-1}, due to a υ(O—O) vibrational mode, and a pair of peaks at 697 and 670 cm^{-1}, arising from the peroxo ring modes of the Fe-(η^2-O_2) unit. The peaks at 550 and 507 cm^{-1} are further assigned to the υ_{asym} and υ_{sym} modes of the iron—oxygen bond of the peroxo species. Similar features are more clearly visible in the ATR spectrum of an oxidized sample (see Figure S15, Supporting Information). Small changes are also visible in the Raman spectrum of the sample upon O_2 interaction (see Figure S16, Supporting Information). Overall, the vibrational spectra are fully consistent with the model already developed from interpretation of the O_2 adsorption data and Mössbauer spectra.

Structures via Neutron Powder Diffraction. Powder neutron diffraction data provide direct structural details of the means by which O_2 and N_2 interact with Fe_2(dobdc) (see Figure 8). Initial data collected on an evacuated sample of Fe_2(dobdc) confirm the presence of accessible Fe^{II} sites with a square pyramidal coordination environment. Here, each iron center is coordinated by O donor atoms from two aryloxide units (located at the front right and back left basal positions) and three carboxylate groups (at the remaining positions) from surrounding dobdc^{4-} ligands. Note that the arrangement of framework O donor atoms is the same in each depiction shown in Figure 8.

A Rietveld refinement was performed against data collected for a sample of Fe_2(dobdc) that was cooled to 100 K, dosed with 2 equivalents of O_2 per iron, and then cooled to 4 K (see Figure S17, Supporting Information). Three different O_2 adsorption sites are evident in the resulting model. The highest occupancy site, with a refined occupancy of 0.917(8) O_2 molecules per iron, is located at the open iron coordination position. Significantly, the O_2 molecule binds in a symmetric side-on coordination mode, with Fe−O distances of 2.09(2) and 2.10(1) Å. The O−O separation of 1.25(1) Å lies between the internuclear distances observed for free O_2 (1.2071(1) Å)[26] and typical of an O_2^- superoxide unit (1.28 Å).[4] This again is consistent with only partial reduction of O_2 under these conditions. Although symmetric side-on coordination of superoxide and peroxide to other transition metals has been reported,[27] this represents, to the best of our knowledge, the first crystallographic evidence of nonbridging side-on binding of any dioxygen species to iron in a nonenzyme system.[28] The second and third O_2 adsorption sites, with occupancies of 0.857(9) and 0.194(8), respectively, occur in the pores of the framework at distances of greater than 3 Å from the iron center and organic linker (see Figure S18, Supporting Information), indicating weak dispersive type interactions between the adsorbate and the framework walls.

Rietveld refinement performed against data collected on a sample of Fe_2(dobdc) that had been dosed with an excess of O_2 at room temperature, evacuated, and subsequently cooled to 4 K was also performed (see Figure S19, Supporting Information). The data were best fit by a model in which O_2 is coordinated to iron in an asymmetric side-on mode and at a refined occupancy of 0.46(2). The model indicates substantial elongation of the O−O distance to 1.6(1) Å, consistent with a two-electron reduction of O_2 to peroxide. With an Fe−O_2 centroid distance of 2.26(1) Å, the peroxide unit also appears to have slipped substantially toward one of the bridging ligands. This type of coordination of peroxide has been observed previously in naphthalene dioxygenase[28a] and has also been proposed based upon spectroscopic evidence for a number of non-heme iron complexes.[29]

Neutron powder diffraction data were further collected on a sample of Fe_2(dobdc) dosed with 0.5, 1.0, and 2.0 equiv of N_2 dosed at 80 K. Upon dosing with approximately 0.5 equiv of N_2, a binding site at the metal center is apparent with an occupancy of 0.641(5). Nitrogen coordinates end on with an Fe−N−N angle of 179(1)° and an Fe−N distance of 2.30(1) Å. The N−N distance of 1.133(15) Å is slightly longer than the N−N distance of free nitrogen (1.0977(1) Å).[30] Additional N_2 uptake reveals a second site that runs more parallel to the pore walls, with N···O contacts between 3.4 and 3.6 Å. The close N_2-framework interactions are the origins of the relatively high enthalpy for adsorption. The metal-specific interactions, however, are clearly much weaker than those for O_2, which results in interaction of both atoms with the metal, electron transfer, and a significant compression of the unit cell upon adsorption (see Table S4, Supporting Information).

The differences in how O_2 binds to iron within Fe_2(dobdc) at low versus high temperatures suggest that the framework undergoes electron transfer processes similar to those reported for non-heme iron-containing enzymes.[12d] In these systems, O_2 typically progresses through a number of electron transfer steps starting with superoxo and peroxo. In the case of Fe_2(dobdc) at low temperature, each iron shares one of its electrons with a single O_2 molecule, resulting in oxidation of all of the metal centers to an intermediate iron(II/III) oxidation state. This charge transfer is reversible at low temperatures and accounts for the high gas uptake demonstrated in the gas adsorption experiments. However, at elevated temperatures, two electrons are transferred to the adsorbing O_2 molecule, the first presumably being shared in a manner analogous to what occurs at low temperature, and the second subsequently arriving from an adjacent iron center by promotion over an activation barrier via the available thermal energy. In this scenario, all of the metal centers within the framework are converted to iron(III), half of which are coordinated irreversibly to a peroxide anion, while the other half remain five-coordinate.

■ CONCLUSIONS AND OUTLOOK

The foregoing results demonstrate the ability of Fe_2(dobdc), a new microporous metal−organic framework with open iron(II) coordination sites, to selectively bind O_2 over N_2 via electron transfer interactions. Breakthrough curves calculated using single-component gas adsorption isotherms and ideal adsorbed solution theory indicate that the material should be capable of the high-capacity separation of O_2 from air at temperatures as high as 226 K. This is substantially higher than the cryogenic temperatures currently used to separate O_2 from air on a large scale. At still greater temperatures, a thermal activation barrier to the formation of iron(III)-peroxide species is overcome and desorption of O_2 is no longer possible. Efforts are underway to synthesize related metal−organic frameworks with an increased activation barrier for the formation of peroxide, thereby generating a high-capacity O_2 separation material that can operate closer to ambient temperatures. In addition, the efficacy of the new redox-active framework in performing a variety of other gas separations where charge transfer might also lead to selectivity is currently under investigation. Finally, given its clear ability to activate O_2, the possibility of employing Fe_2(dobdc) as a catalyst for the oxidation of hydrocarbons by air will be explored.

■ ASSOCIATED CONTENT

Ⓢ Supporting Information. Additional experimental details, including two movie files. This material is available free of charge via the Internet at http://pubs.acs.org.

■ AUTHOR INFORMATION

Corresponding Author
jrlong@berkeley.edu

■ ACKNOWLEDGMENT

This research was supported through the Center for Gas Separations Relevant to Clean Energy Technologies, an Energy Frontier Research Center funded by the U.S. Department of Energy, Office of Science, Office of Basic Energy Sciences under Award No. DE-SC0001015. W.L.Q. gratefully acknowledges the NIST NRC Postdoctoral Fellowship Research Associateship program. We thank L. Valenzano and B. Civalleri for their help in the assignment of the infrared spectrum through the animation of vibrational modes of the optimized framework structure with CRYSTAL code and F. Bonino for Raman contributions.[31]

REFERENCES

(1) Ermsley, J. *Oxygen, Nature's Building Blocks: An A-Z Guide to the Elements*; Oxford University Press: Oxford, England, 2001.

(2) (a) Schütz, M.; Daun, M.; Weinspach, P.-M.; Krumbeck, M.; Hein, K. R. G. *Energy Convers. Manage.* **1992**, *33*, 357. (b) Descamps, C.; Bouallou, C.; Kannich, M. *Energy* **2008**, *33*, 874.

(3) (a) Hadjipaschalis, I.; Kourtis, G.; Poullikkas, A. *Renewable Sustainable Energy Rev.* **2009**, *13*, 2637. (b) Kather, A.; Scheffknecht, G. *Naturwissenschaften* **2009**, *96*, 993.

(4) Greenwood, N. N.; Earnshaw, A. *Chemistry of the Elements*, 2nd ed.; Butterworth Heinemann: Burlington, MA, 2002; pp 604, 616.

(5) Nandi, S. P.; Walker, P. L., Jr. *Sep. Sci. Technol.* **1976**, *11*, 441.

(6) (a) Eddaoudi, M.; Kim, J.; Rosi, N.; Vodak, D.; Wachter, J.; O'Keeffe, M.; Yaghi, O. M. *Science* **2002**, *295*, 469. (b) Kitagawa, S.; Kitaura, R.; Noro, S.-I. *Angew. Chem., Int. Ed.* **2004**, *43*, 2334. (c) Matsuda, R.; Kitaura, R.; Kitagawa, S.; Kubota, Y.; Belosludov, R. V.; Kobayashi, T. C.; Sakamoto, H.; Chiba, T.; Takata, M.; Kawazoe, Y.; Mita, Y. *Nature* **2005**, *436*, 238. (d) Millward, A. R.; Yaghi, O. M. *J. Am. Chem. Soc.* **2005**, *127*, 17998. (e) Furukawa, H.; Miller, M. A.; Yaghi, O. M. *J. Mater. Chem.* **2007**, *17*, 3197. (f) Férey, G. *Chem. Soc. Rev.* **2008**, *37*, 191. (g) Ma, S.; Sun, D.; Simmons, J. M.; Collier, C. D.; Yuan, D.; Zhou, H.-C. *J. Am. Chem. Soc.* **2008**, *130*, 1012. (h) Morris, R. E.; Wheatley, P. S. *Angew. Chem., Int. Ed.* **2008**, *47*, 4966. (i) Llewellyn, P. L.; Bourrelly, S.; Serre, C.; Vimont, A.; Daturi, M.; Hamon, L.; De Weireld, G.; Chang, J.-S.; Hong, D.-Y.; Hwang, Y. K.; Jhung, S. H.; Férey, G. *Langmuir* **2008**, *24*, 7245. (j) Murray, L. J.; Dincă, M.; Long, J. R. *Chem. Soc. Rev.* **2009**, *38*, 1294. (k) Chen, B.; Xiang, S.; Qian, G. *Acc. Chem. Res.* 2010, *43*, 1115.

(7) (a) Hayashi, H.; Côté, A. P.; Furukawa, H.; O'Keeffe, M.; Yaghi, O. M. *Nat. Mater.* **2007**, *6*, 501. (b) Britt, D.; Tranchemontagne, D.; Yaghi, O. M. *Proc. Natl. Acad. Sci. U.S.A.* **2008**, *105*, 11623. (c) Britt, D.; Furukawa, H.; Wang, B.; Glover, T. G.; Yaghi, O. M. *Proc. Natl. Acad. Sci. U.S.A.* **2009**, *106*, 20637. (d) Li, J.-R.; Kuppler, R. J.; Zhou, H.-C. *Chem. Soc. Rev.* **2009**, *38*, 1477.

(8) (a) Mulfort, K. L.; Hupp, J. T. *J. Am. Chem. Soc.* **2007**, *129*, 9604. (b) Ingleson, M. J.; Perez Barrio, J.; Guilbaud, J. B.; Khimyak, Y. Z.; Rosseinsky, M. J. *Chem. Commun.* **2008**, 2680. (c) Doonan, C. J.; Morris, W.; Furukawa, H.; Yaghi, O. M. *J. Am. Chem. Soc.* **2009**, *131*, 9492. (d) Tanabe, K. K.; Cohen, S. M. *Angew. Chem., Int. Ed.* **2009**, *48*, 7424.

(9) (a) Seo, J. S.; Whang, D.; Lee, H.; Jun, S. I.; Oh, J.; Jeon, Y. J.; Kim, K. *Nature* **2000**, *404*, 982. (b) Wu, C.-D.; Hu, A.; Zhang, L.; Lin, W. *J. Am. Chem. Soc.* **2005**, *127*, 8940. (c) Bloch, E. D.; Britt, D.; Lee, C.; Doonan, C. J.; Uribe-Romo, F. J.; Furukawa, H.; Long, J. R.; Yaghi, O. M. *J. Am. Chem. Soc.* **2010**, *132*, 14382. (d) Chavan, S.; Vitillo, J. G.; Uddin, M. J.; Bonino, F.; Lamberti, C.; Groppo, E.; Lillerud, K.-P.; Bordiga, S. *Chem. Mater.* **2010**, *22*, 4602.

(10) (a) Rosi, N. L.; Kim, J.; Eddaoudi, M.; Chen, B.; O'Keeffe, M.; Yaghi, O. M. *J. Am. Chem. Soc.* **2005**, *127*, 1504. (b) Dietzel, P. D. C.; Morita, Y.; Blom, R.; Fjellvåg, H. *Angew. Chem., Int. Ed.* **2005**, *44*, 6354. (c) Dietzel, P. D. C.; Panella, B.; Hirscher, M.; Blom, R.; Fjellvåg, H. *Chem. Commun.* **2006**, 959. (d) Caskey, S. R.; Wong-Foy, A. G.; Matzger, A. J. *J. Am. Chem. Soc.* **2008**, *130*, 10870. (e) Zhou, W.; Wu, J.; Yildirim, T. *J. Am. Chem. Soc.* **2008**, *130*, 15268. (f) Dietzel, P. D. C.; Johnsen, R. E.; Blom, R.; Fjellvåg, H. *Chem.—Eur. J.* **2008**, *14*, 2389. (g) Dietzel, P. D. C.; Blom, R.; Fjellvåg, H. *Eur. J. Inorg. Chem.* **2008**, 3624. (h) Bhattacharjee, S.; Choi, J.; Yang, S.; Choi, S. B.; Kim, J.; Ahn, W. *J. Nanosci. Nanotechnol.* **2010**, *10*, 135. (i) Lamberti, C.; Zecchina, A.; Groppo, E.; Bordiga, S. *Chem. Soc. Rev.* **2010**, *39*, 4951. (j) Valenzano, L.; Civalleri, B.; Chavan, S.; Palomino, G. T.; Areán, C. O.; Bordiga, S. *J. Phys. Chem. C* **2010**, *114*, 11185.

(11) (a) Chui, S. S. Y.; Lo, S. M. F.; Charmant, J. P. H.; Orpen, A. G.; Williams, I. D. *Science* **1999**, *283*, 1148. (b) Kramer, M.; Schwarz, U.; Kaskel, S. *J. Mater. Chem.* **2006**, *16*, 2245. (c) Murray, L. J.; Dincă, M.; Yano, J.; Chavan, S.; Bordiga, S.; Brown, C. M.; Long, J. R. *J. Am. Chem. Soc.* **2010**, *132*, 7856.

(12) (a) Feig, A. L.; Lippard, S. J. *Chem. Rev.* **1994**, *94*, 759. (b) Que, L.; Dong, Y. *Acc. Chem. Res.* **1996**, *29*, 190. (c) Sono, M.; Roach, M. P.; Coulter, E. D.; Dawson, J. H. *Chem. Rev.* **1996**, *96*, 2841. (d) Kovaleva, E. G.; Neibergall, M. B.; Chakrabarty, S.; Lipscomb, J. D. *Acc. Chem. Res.* **2007**, *40*, 475.

(13) Liss, K.-D.; Hunter, B. A.; Hagen, M. E.; Noakes, T. J.; Kennedy, S. J. *Phys. B* **2006**, *385*−*386*, 1010.

(14) (a) Toby, B. H. *J. Appl. Crystallogr.* **2001**, *34*, 210. (b) Larson, A. C.; Von Dreele, R. B. *Los Alamos National Laboratory Report LAUR* **1994**, 86–748.

(15) (a) Halder, G. J.; Chapman, K. W.; Neville, S. M.; Moubaraki, B.; Murray, K. S.; Létard, J.-F.; Kepert, C. J. *J. Am. Chem. Soc.* **2008**, *130*, 17552. (b) Ma, S.; Yuan, D.; Chang, J.-S.; Zhou, H.-C. *Inorg. Chem.* **2009**, *48*, 5398. (c) Sumida, K.; Horike, S.; Kaye, S. S.; Herm, Z. R.; Queen, W. L.; Brown, C. M.; Grandjean, F.; Long, G. J.; Dailly, A.; Long, J. R. *Chem. Sci.* **2010**, *1*, 184. (d) Nayak, S.; Harms, K.; Dehnen, S. *Inorg. Chem.* **2010**, *50*, 2714.

(16) Dietzel, P. D. C.; Georgiev, P. A.; Eckert, J.; Blom, R.; Strässle, T.; Unruh, T. *Chem. Commun.* **2010**, *46*, 4962.

(17) Figgis, B. N. *Introduction to Ligand Fields*; John Wiley & Sons Inc.: New York, 1967.

(18) Sherman, D. M. *Am. Mineral.* **1985**, *70*, 1262.

(19) (a) Li, Y.; Yang, R. T. *Langmuir* **2007**, *23*, 12937. (b) Maji, T. K.; Matsuda, R.; Kitagawa, S. *Nat. Mater.* **2007**, *6*, 142. (c) Yoon, J. W.; Jhung, S. H.; Hwang, Y. K.; Humphrey, S. M.; Wood, P. T.; Chang, J.-S. *Adv. Mater.* **2007**, *19*, 1830. (d) Mu, B.; Schoenecker, P. M.; Walton, K. S. *J. Phys. Chem. C* **2010**, *114*, 6464. (e) Xue, M.; Zhang, Z.; Xiang, S.; Jin, Z.; Liang, C.; Zhu, G.-S.; Qiu, S.-L.; Chen, B. *J. Mater. Chem.* **2010**, *20*, 3984. (f) Bae, Y.-S.; Spokoyny, A. M.; Farha, O. K.; Snurr, R. Q.; Hupp, J. T.; Mirkin, C. A. *Chem. Commun.* **2010**, *46*, 3478. (g) Southon, P. D.; Price, D. J.; Nielsen, P. K.; McKenzie, C. J.; Kepert, C. J. *J. Am. Chem. Soc.* **2011**, *133*, 10885.

(20) Krishna, R.; Long, J. R. *J. Phys. Chem. C* **2011**, *115*, 12941.

(21) (a) Kumar, R. *Sep. Sci. Technol.* **1996**, *31*, 877. (b) Jee, J.-G.; Lee, J.-S.; Lee, C.-H. *Ind. Eng. Chem. Res.* **2001**, *40*, 3647.

(22) Ingalls, A. *Phys. Rev.* **1964**, *A133*, 787.

(23) (a) Shenoy, G. K.; Wagner, F. E.; Kalvius, G. M. *Mössbauer Isomer Shifts*; Shenoy, G. K., Wagner, F. E., Eds.; North-Holland: Amsterdam, 1978; p 49. (b) Owen, T.; Grandjean, F.; Long, G. J.; Domasevitch, K. V.; Gerasimchuk, N. *Inorg. Chem.* **2008**, *47*, 8704 and references given therein.

(24) (a) Vaska, L. *Acc. Chem. Res.* **1976**, *9*, 175. (b) Watanabe, T.; Ama, T.; Nakamoto, K. *J. Phys Chem.* **1984**, *88*, 440–445. (c) Zecchina, A.; Scarano, D.; Spoto., G. *J. Mol. Catal.* **1986**, *38*, 287–293. (d) Liu, J.; Ohta, T.; Yamaguchi, S.; Ogura, T.; Sakamoto, S.; Maeda, Y.; Naruta, Y. *Angew. Chem., Int. Ed.* **2009**, *48*, 9262.

(25) (a) Ahmad, S.; McCallum, J. D.; Shiemke, A. K.; Appelman, E. H.; Loehr, T. M.; Sanders-Loehr, J. *Inorg. Chem.* **1988**, *27*, 2230. (b) McCandlish, E.; Miksztal, A. R.; Nappa, M.; Sprenger, A. Q.; Valentine, J. S.; Stong, J. D.; Spiro, T. G. *J. Am. Chem. Soc.* **1980**, *102*, 4268.

(26) Babcock, H. D.; Herzberg, L. *Astrophys. J.* **1948**, *108*, 167.

(27) (a) Stomberg, R.; Ainalem, I. -B. *Acta Chem. Scand.* **1968**, *22*, 1439. (b) Van Atta, R. B.; Strouse, C. E.; Hanson, L. K.; Valentine, J. S. *J. Am. Chem. Soc.* **1987**, *109*, 1425. (c) Egan, J. W., Jr.; Haggerty, B. S.; Rheingold, A. L.; Sendlinger, S. C.; Theopold, K. H. *J. Am. Chem. Soc.* **1990**, *112*, 2445. (d) Yao, S.; Bill, E.; Milsmann, C.; Wieghardt, K.; Driess, M. *Angew. Chem., Int. Ed.* **2008**, *47*, 7110. (e) Cho, J.; Sarangi, R.; Annaraj, J.; Kim, S. Y.; Kubo, M.; Ogura, T.; Solomon, E. I.; Nam., W. *Nat. Chem.* **2009**, *1*, 568. (f) Annaraj, J.; Cho, J.; Lee, Y. -M.; Kim, S. Y.; Latifi, R.; de Visser, S. P.; Nam, W. *Angew. Chem., Int. Ed.* **2009**, *48*, 4150.

(28) (a) Karlsson, A.; Parales, J. V.; Parales, R. E.; Gibson, D. T.; Eklund, H.; Ramaswamy, S. *Science* **2003**, *299*, 1039. (b) Kovaleva, E. G.; Lipscomb, J. D. *Science* **2007**, *316*, 453.

(29) (a) Roelfes, G.; Vrajmasu, V.; Chen, K.; Ho, R. Y. N.; Rohde, J.-U.; Zondervan, C.; la Crois, R. M.; Schudde, E. P.; Lutz, M.; Spek, A. L.; Hage, R.; Feringa, B. L.; Münck, E.; Que, L., Jr. *Inorg. Chem.* **2003**, *42*, 2639. (b) Horner, O.; Mouesca, J.-M.; Oddou, J.-L.; Jeandey, C.; Nivière, V.; Mattioli, T. A.; Mathé, C.; Fontecave, M.; Maldivi, P.; Bonville, P.; Halven, J. A.; Latour, J.-M. *Biochemistry* **2004**, *43*, 8815.

(30) Huber, K. P.; Herzberg, G. *Molecular Spectra and Molecular Structure. IV. Constants of Diatomic Molecules*; Van Nostrand Reinhold: New York, 1979; p 420.

(31) Certain trade names and company products are mentioned in this paper to adequately specify the experimental procedure and equipment used. In no case does this imply recommendation or endorsement by NIST, nor does it imply that the products are necessarily the best available for this purpose.